minerals

MDPI

Article

Geochemical and Mineralogical Characteristics of Ion-Adsorption Type REE Mineralization in the Mosuoying Granite, Panxi Area, Southwest China

Ling Gan [1], Bing Yan [1,*], Yuqing Liu [2], Yan Gao [1], Chuan Yin [3], Liye Zhu [1], Shuang Tan [1], Di Ding [1] and Haiyun Jiang [4]

[1] College of Earth Science, Chengdu University of Technology, Chengdu 610059, China; ganling@stu.cdut.edu.cn (L.G.)
[2] School of Construction Management, Chongqing Jianzhu College, Chongqing 400060, China
[3] Sichuan Geological and Mineral Group Co., Ltd., Chengdu 610036, China
[4] Sichuan Xingye Geotechnical Engineering Detecting Co., Ltd., Chengdu 610084, China
* Correspondence: yanbingcdut@outlook.com

Abstract: The ion-adsorption rare earth deposit developed on the Mosuoying granite in the Panxi area of southwestern China represents a significant advancement in the exploration of ion-adsorption rare earth deposits in Sichuan. Being the first and currently the sole ion-adsorption rare earth deposit in Sichuan, studying its rare earth mineralization characteristics holds great importance. This paper aims to investigate the geochemical properties of the Mosuoying granite and its overlying weathered crust using rock geochemical methods based on field geological investigations. The findings reveal that the deposit belongs to the light rare earth type, with the ore-forming parent rock attributed to the high-potassium calc-alkaline series. It exhibits a high rock REE content ranging from 419 to 578 ppm, indicating favorable mineralization potential. Hydrothermal alteration reduces the REE content of the parent rock, leading to a notable increase in the LREE/HREE ratio, thus impacting the partitioning of rare earth elements and subsequent ore formation. The distribution characteristics of rare earth elements in each layer of the weathered crust are controlled by the parent rock and exhibit a light rare earth distribution pattern. The completely weathered layer is the main enrichment zone for rare earth elements, and the migration and enrichment patterns of rare earth elements in the weathered crust are evident. From the semi-weathered layer to the completely weathered layer, all REEs were gained, with a higher degree of migration for LREE. From the completely weathered layer to the clay layer, all REEs were lost, and the vertical distribution of rare earth content shows a "low-high-low" pattern.

Keywords: ion-adsorption type REE deposit; weathering crust; Mosuoying granite; REE migration and enrichment; Southwest China

Citation: Gan, L.; Yan, B.; Liu, Y.; Gao, Y.; Yin, C.; Zhu, L.; Tan, S.; Ding, D.; Jiang, H. Geochemical and Mineralogical Characteristics of Ion-Adsorption Type REE Mineralization in the Mosuoying Granite, Panxi Area, Southwest China. *Minerals* **2023**, *13*, 1449. https://doi.org/10.3390/min13111449

Academic Editor: Argyrios Papadopoulos

Received: 23 September 2023
Revised: 17 October 2023
Accepted: 5 November 2023
Published: 17 November 2023

1. Introduction

Ion-adsorption rare earth deposits (iREEs) have been widely studied as a significant source of heavy rare earth elements [1–5]. These deposits were first discovered in Jiangxi province in the late 1960s, and similar occurrences have since been found in other provinces in southern China [6]. However, exploration and research over the past few decades have only identified these deposit types in seven southern provinces (Jiangxi, Guangdong, Guangxi, Fujian, Hunan, Yunnan, and Zhejiang), suggesting a limited regional distribution of ionic adsorption deposits.

Sichuan, known for its considerable reserves and status as a major producer of rare earth elements, has gained global attention due to its Maoniuping and Dalucao rare earth mines located in the Mianning-Dechang REE metallogenic belt [7,8]. Unfortunately, these carbonate-type rare earth deposits primarily yield light rare earth resources, with limited production of the more valuable heavy rare earth resources. Despite favorable climatic

and topographic conditions for the development of ion-adsorption rare earth deposits and extensive exploration efforts, no such deposits were found in Sichuan [9,10]. Exploration for this particular type of deposit in Sichuan was halted in the 1990s. However, as our understanding of ore deposit theories and exploration techniques deepened, ion-adsorption rare earth deposits were subsequently discovered in Hunan [11], Hainan [12], Anhui [13], and other regions [14]. This prompted Sichuan to resume exploration efforts, ultimately leading to the discovery of these deposits above the Mosuoying granite body in the western part of the province [15,16]. This significant finding expanded the prospects for ionic adsorption rare earth deposits in China. Mosuoying granite is currently the oldest known ion adsorption type rare earth ore-forming parent rock [17].

In order to study the genesis of this deposit, it is essential to clarify the geochemical characteristics of the weathered crust profile. This article analyzes the mineralogical and geochemical properties of the parent rock and weathered crust through mineralogical and geochemical research and further discusses the migration and enrichment patterns of ore-forming elements and the controlling factors of mineralization. The aim is to provide a theoretical basis for understanding the origin of this deposit.

2. Geological Background

The research area is located in the Mianning-Dechang REE metallogenic belt in Sichuan. The basement consists of Archean high-grade metamorphic rocks, Proterozoic metamorphic sedimentary rocks, and overlying Phanerozoic clastic rocks and carbonate rocks. The tectonic location belongs to the western margin of the Yangtze craton, within the Kangdian basement uplift zone of the Kangdian foreland thrust belt of the Up-Yangtze ancient continental block, on the Anning River fault zone in the middle section of the west Sichuan central Yunnan oldland [18]. The Kangdian basement uplift zone is a horst uplift belt composed of banded distributions of Proterozoic to Early Mesozoic metamorphic and magmatic complex rocks. Among them, the Jingningian (~1080 Ma) granite rocks and Chengjiang (~530 Ma) magmatic rocks are widely distributed. The direction of the tectonic line is nearly north-south, and the direction of the uplift is controlled by the north-south fault belt (Figure 1).

The ore-forming parent rock is the Mosuoying granite body, which is distributed along the Dechang-Miyi line, showing a flat circular north-south distribution. It has a length of about 35 km from north to south, a width of about 10 km from east to west, and covers an area of about 330 km^2. The formation age of the rock mass spans a large time range, with zircon U-Pb isotopic ages of 1055 $\pm$ 43 Ma [19] and 803–790 Ma [20], indicating that the rock formed after the Jingningian period. It includes three main rock units: Kelang, Yonglang, and Maoping, representing multiple magma emplacement events. The rock mass is in intrusive contact with the surrounding rocks and commonly undergoes thermal contact metamorphism. The minerals at the edges gradually become finer, sometimes showing cold condensation rims [17]. Diabase dikes can be observed in the region, indicating a tectonic environment of extension and stretching after diagenesis.

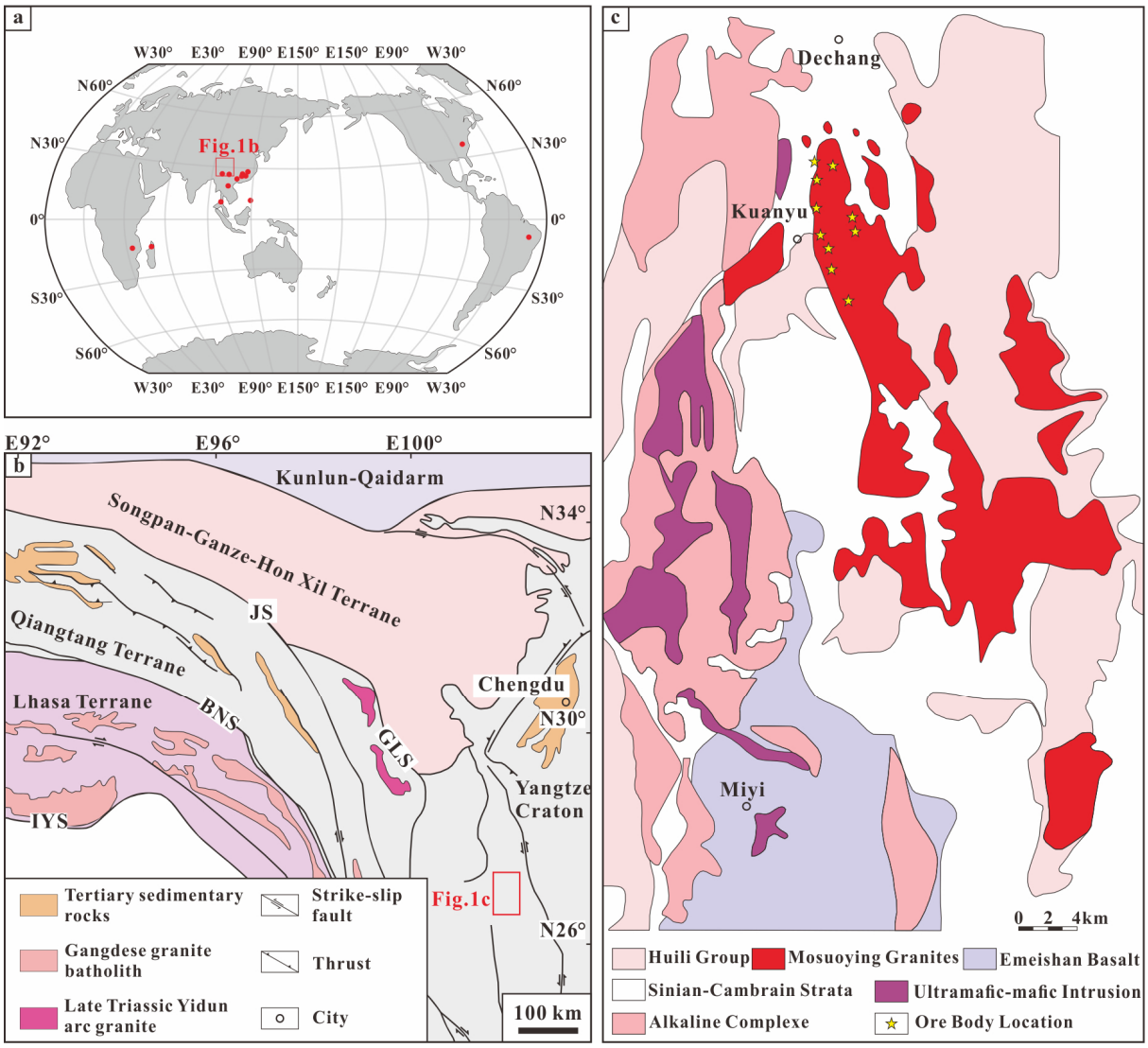

Figure 1. Regional Geological Map. (**a**) Global distribution of regolith-hosted REE deposits and prospects [21]; (**b**) simplified tectonic map of the Himalayan-Tibetan Orogen [22]; (**c**) the distribution of Mosuoying granite [17].

3. Sampling and Analytical Methods

3.1. Profile Characteristics and Sampling Strategy

The sampling site is located in Kuanyu Township, Dechang County, Sichuan Province, southwest China. It is situated in a subtropical region characterized by a hot climate, abundant rainfall, well-developed vegetation, and diverse topography. The terrain consists of typical Zhongshan mountainous terrain and limited river valley terrain, exhibiting complex and diverse landforms.

Based on color, weathering degree, and structural characteristics, the weathering profile in the study area is divided into five layers: the humic layer, clay layer, completely weathered layer, semi-weathered layer, and bedrock layer (Figure 2). The humic layer is typically yellow and turns yellow-brown when the organic matter content is high. The clay layer is brick-red in color, with a heavy texture and poor permeability and air permeability. The primary granite has undergone nearly complete decomposition, with only a small amount of fine quartz remaining. The completely weathered layer has a loose structure and good soil permeability. From top to bottom, the soil color changes from brick-red to gray-white. The semi-weathered layer has a loose and fragile structure and contains some

partially weathered granite. The bedrock layer is predominantly composed of physically fragmented rocks.

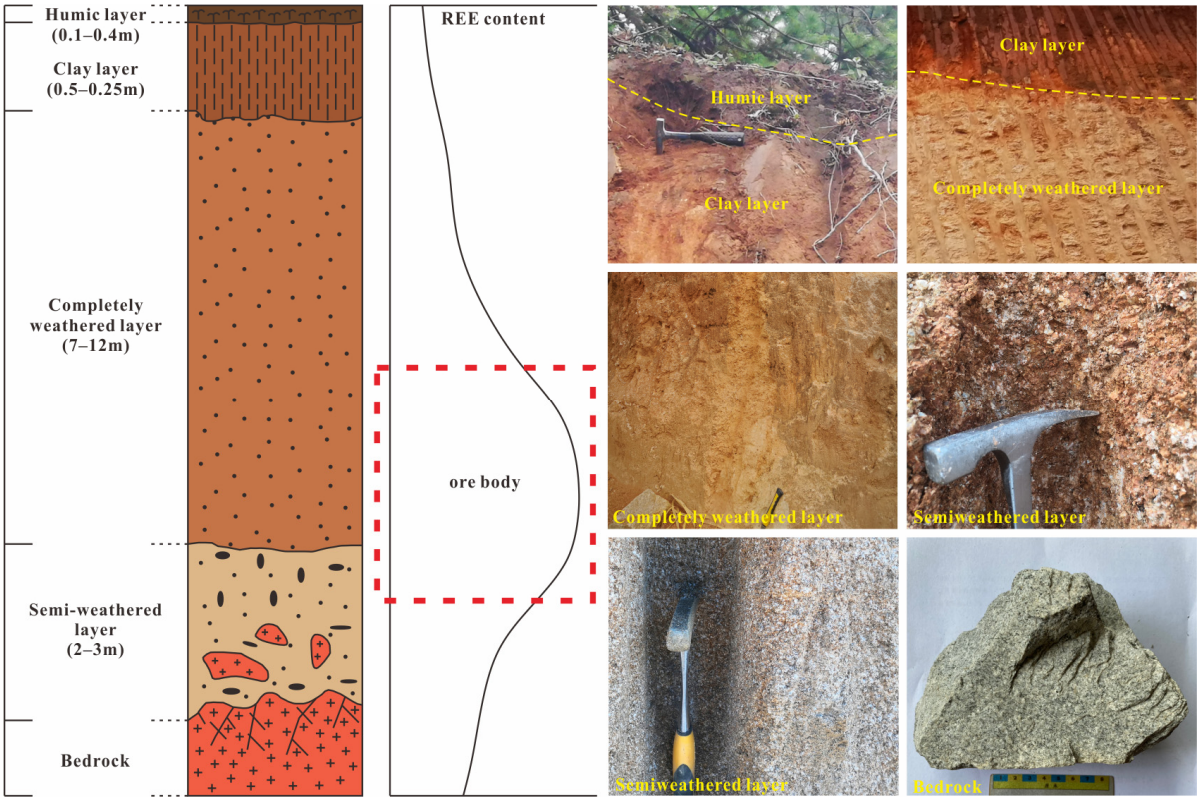

Figure 2. Schematic profile of the Mosuoying granite REE deposit and the variation of REE concentration along profile [21,23].

A total of 17 representative samples were collected from selected profiles in the area. This includes one sample from the humic layer (A1), five samples from the clay layer (B1–B5), five samples from the completely weathered layer (C1–C5), three samples from the semi-weathered layer (D1–D3), and three samples from the bedrock layer (E1–E2 representing fresh bedrock and E3 showing alteration, characterized by greisenization).

3.2. Analytical Methods

Bedrock petrography was studied with a polarizing microscope (OPTIPHOT-POL, manufactured by Nikon, Tokyo, Japan) using plane-polarized light and perpendicularly polarized light. The backscattered electron (BSE) images of weathering crust samples were taken using a scanning electron microscope (SEM, NANO SEM450, manufactured by Thermo Fisher Scientific, Waltham, MA, USA) equipped with an energy dispersive X-ray spectrometer (EDS). The mineral compositions of the samples were measured using a Bruker D8 Advance X-ray diffractometer (manufactured by Bruker, Billerica, MA, USA) between 3° and 70° (2θ) at scanning speed of 3° min^{-1} with Cu Kα radiation (40 mA and 40 kV). The XRD data were processed by DIFFRAC.EVA V3.1 software.

Major-element analyses of whole-rock samples from the Mosuoying granite were determined using an X-ray fluorescence spectrometer (PW4400). The analytical precision is better than 5% for all the major elements; the results are listed in Table 1. The concentrations of trace elements, including those of REEs, were analyzed using a PlasmaQuant-MS Elite inductively coupled plasma mass spectrometer (ICP-MS). The relative standard deviation of the repeatability test for analysis is better than 10%; the results are listed in Table 2.

Table 1. Major elements (wt.%) compositions of the studied samples from the weathering crust.

Layer	Humic			Clay			Completely Weathered					Semi-Weathered			Bedrock		
Sample	**A1**	**B1**	**B2**	**B3**	**B4**	**B5**	**C1**	**C2**	**C3**	**C4**	**C5**	**D1**	**D2**	**D3**	**E1**	**E2**	**E3**
SiO_2	57.17	58.00	48.30	57.37	56.57	56.15	55.58	57.21	68.89	64.45	69.70	72.26	64.31	67.96	70.65	70.45	74.62
Al_2O_3	18.17	21.31	27.11	22.90	23.31	23.29	19.90	22.45	17.24	18.61	16.78	14.36	19.13	17.51	14.72	14.36	12.32
Fe_2O_3	4.98	5.81	7.95	6.04	6.07	5.24	8.55	4.27	2.58	3.35	2.40	2.56	3.42	2.46	2.34	3.71	2.95
MgO	0.68	0.67	0.58	0.33	0.42	0.56	2.19	0.47	0.24	0.45	0.09	0.14	0.47	0.42	0.34	0.47	0.18
CaO	0.26	0.25	0.15	0.12	0.12	0.16	1.02	0.17	0.14	0.24	0.09	0.27	0.19	0.18	1.46	1.74	0.57
Na_2O	0.70	0.43	0.74	0.32	0.36	0.38	0.32	0.44	0.35	0.81	0.50	1.26	0.46	0.41	3.13	3.1	2.55
K_2O	4.50	4.89	3.38	4.77	5.08	6.29	3.96	5.95	6.38	6.76	6.95	6.67	6.51	5.57	6.02	4.52	5.25
MnO	0.174	0.044	0.021	0.021	0.031	0.022	0.106	0.023	0.013	0.021	0.012	0.020	0.030	0.021	0.018	0.031	0.025
P_2O_5	0.179	0.095	0.070	0.064	0.056	0.071	0.074	0.083	0.045	0.100	0.057	0.051	0.080	0.056	0.098	0.145	0.065
TiO_2	0.647	0.676	0.912	0.503	0.545	0.705	1.013	0.661	0.306	0.516	0.106	0.207	0.591	0.342	0.193	0.386	0.182
S	0.042	0.008	0.012	0.019	0.007	0.021	0.029	0.010	0.010	0.022	0.015	0.018	0.024	0.018	0.0131	0.0127	0.0127
LOI	11.79	7.65	11.02	7.01	6.63	6.85	6.53	7.66	3.72	4.00	3.18	1.87	4.61	4.42	0.24	0.32	0.51
SUM	99.19	99.84	100.24	99.47	99.20	99.74	99.28	99.40	99.92	99.32	99.88	99.68	99.82	99.36	99.22	99.25	99.24
CIA	76.89	79.28	86.39	81.47	80.74	77.32	78.97	77.39	71.51	70.44	69.00	63.65	72.77	73.98	58.11	60.54	59.55

$CIA = [Al_2O_3/(Al_2O_3 + CaO + Na_2O + K_2O)] \times 100$.

Table 2. Trace elements and REEs (ppm) compositions of the studied samples from the weathering crust.

Layer	Humic			Clay			Completely Weathered					Semi-Weathered			Bedrock		
Sample	**A1**	**B1**	**B2**	**B3**	**B4**	**B5**	**C1**	**C2**	**C3**	**C4**	**C5**	**D1**	**D2**	**D3**	**E1**	**E2**	**E3**
Rb	343.0	356.0	270.0	335.0	271.0	385.0	462.0	426.0	404.0	364.0	410.0	495.0	335.0	412	406.0	338.0	373.0
Sr	49.3	35.8	59.2	46.9	47.0	76.0	71.7	26.8	25.9	21.4	57.0	63.2	45.7	27.5	37.9	79.8	81.9
Y	46.0	139.0	41.1	77.4	42.6	40.3	35.5	171.0	110.0	124.0	76.7	89.6	48.8	56.8	90.5	93.1	33.9
Zr	231.0	442.0	191.0	264.0	359.0	553.0	365.0	215.0	258.0	294.0	615.0	666.0	243.0	228	255.0	282.0	212.0
Nb	20.8	19.7	14.9	25.6	30.4	33.7	26.0	12.9	16.6	20.1	28.9	27.6	30.1	10.8	12.6	13.1	25.2
Ba	350.0	405.0	1029.0	433.0	448.0	683.0	854.0	350.2	493.0	327.1	561.0	769.0	593.0	501	227	796	442
La	32.3	100.0	46.1	91.1	92.0	107.0	138.0	95.3	167.0	181.0	169.0	203.0	109.0	111	119	89.0	111
Ce	105.0	162.0	86.2	143.0	161.0	183.0	215.0	160.0	251.0	309.0	282.0	318.0	159.0	198	197	140	161
Pr	16.2	18.1	9.8	14.8	19.6	19.0	23.6	17.9	27.0	32.3	29.5	34.5	15.9	19.1	21.9	15.4	16.6
Nd	38.5	71.2	37.5	55.2	74.0	71.0	85.5	69.0	103.0	122.0	113.0	130.0	56.2	71.7	78.6	58.9	58.9
Sm	13.3	15.7	8.2	11.7	13.8	13.4	15.5	16.6	20.1	24.3	21.0	24.3	10.8	14.1	16.7	13.2	11.6
Eu	1.7	1.6	1.3	1.3	1.5	1.4	1.0	1.0	1.3	1.6	1.6	1.5	1.0	0.6	0.552	1.13	0.907
Gd	12.7	15.9	7.6	10.3	11.2	10.2	10.9	18.2	17.6	21.0	15.4	18.0	9.1	11.8	13.8	12.2	9.03
Tb	2.1	2.8	1.2	1.7	1.6	1.5	1.5	3.2	2.7	3.1	2.2	2.5	1.4	1.8	2.36	2.04	1.31
Dy	8.5	18.1	7.6	10.4	8.7	8.1	7.6	22.4	15.8	18.3	11.5	13.2	8.1	10.1	14.3	12.4	6.84
Ho	2.5	4.0	1.6	2.1	1.7	1.6	1.4	4.8	3.1	3.6	2.2	2.6	1.6	1.9	2.82	2.54	1.20
Er	3.5	11.3	4.5	6.0	4.5	4.2	3.6	13.6	8.3	9.8	6.0	7.0	4.6	5.2	7.72	6.89	3.07
Tm	0.9	1.6	0.7	0.9	0.6	0.6	0.5	1.9	1.2	1.4	0.9	1.0	0.7	0.7	1.15	0.989	0.436
Yb	3.5	9.9	4.3	5.6	3.9	4.2	3.4	11.6	7.1	8.8	5.7	6.7	4.4	4.5	7.37	6.23	2.77
Lu	0.8	1.4	0.6	0.8	0.6	0.6	0.5	1.6	1.0	1.3	0.8	1.0	0.6	0.6	1.04	0.890	0.408
Hf	7.1	12.6	5.8	8.2	10.5	12.1	10.1	8.5	8.8	9.9	14.3	14.0	7.7	8	9.40	8.73	6.17
Ta	2.3	2.2	1.6	2.8	2.7	2.4	2.3	1.6	1.8	2.2	3.2	2.2	3.7	1.2	1.74	1.43	2.36
Th	31.7	43.6	24.5	42.0	54.7	83.8	65.5	46.9	66.7	118.0	109.0	123.0	56.3	58.3	77.7	36.5	49.9
U	7.4	8.7	5.5	8.6	8.3	9.0	14.8	8.5	10.4	11.9	10.7	10.4	10.2	7.2	10.3	6.44	5.35
∑REE	256.3	531.1	238.1	405.1	411.0	443.5	517.1	555.3	687.5	803	700.1	807.4	408.5	477.5	574.8	454.9	419.0
∑LREE	192.0	351.3	179.6	304.1	346.6	380.0	462.1	342.2	548.0	644.3	593.5	685.5	340.1	399.8	447.6	329.8	369.0
∑HREE	64.3	179.8	58.5	101.0	64.4	63.5	55.0	213.1	139.5	158.7	106.6	121.9	68.4	77.7	127.3	125.1	49.9
∑LREE/ ∑HREE	2.99	1.95	3.07	3.01	5.38	5.98	8.40	1.61	3.93	4.06	5.57	5.62	4.97	5.15	3.52	2.64	7.39
$(La/Yb)_N$	6.6	7.3	7.7	11.6	16.9	18.4	29.0	5.9	16.9	14.8	21.4	21.9	17.6	17.7	11.6	10.3	28.7
$(La/Sm)_N$	1.6	4.1	3.6	5.0	4.3	5.2	5.7	39.4	69.1	74.9	69.9	84.0	45.1	45.9	4.6	4.35	6.18
$(Gd/Yb)_N$	3.0	1.3	1.5	1.5	2.4	2.0	2.6	1.3	2.1	2.0	2.3	2.2	1.7	2.2	1.55	1.62	2.70
Nb/Ta	9.04	8.95	9.31	9.14	11.26	14.04	11.30	8.06	9.22	9.14	9.03	12.55	8.14	9.00	7.24	9.16	10.68
Zr/Hf	32.54	35.08	32.93	32.20	34.19	45.70	36.14	25.29	29.32	29.70	43.01	45.75	31.56	28.50	27.13	32.30	34.36
δEu	0.39	0.31	0.50	0.35	0.36	0.35	0.22	0.18	0.21	0.21	0.26	0.21	0.30	0.14	0.11	0.27	0.26
δCe	1.10	0.85	0.93	0.85	0.87	0.90	0.83	0.87	0.82	0.90	0.89	0.84	0.82	0.95	0.88	0.85	0.82

$(La/Yb)_N$, where N is normalised by chondrite.

4. Results

4.1. Mineral Composition

The bedrock of the weathered crust is biotite granite, with the main mineral composition being quartz (35%), plagioclase (35%), K-feldspar (20%), biotite (5%), and a small amount of accessory minerals (Figure 3a–e). It exhibits varying degrees of alteration and shows a weakly fractured structure (Figure 3e). The small amount of rare earth accessory minerals (apatite, zircon, etc.) is usually the main source of rare earth materials in the deposit, while feldspar and biotite have relatively low REE content and provide only a small contribution to the deposit during the weathering cycle [24].

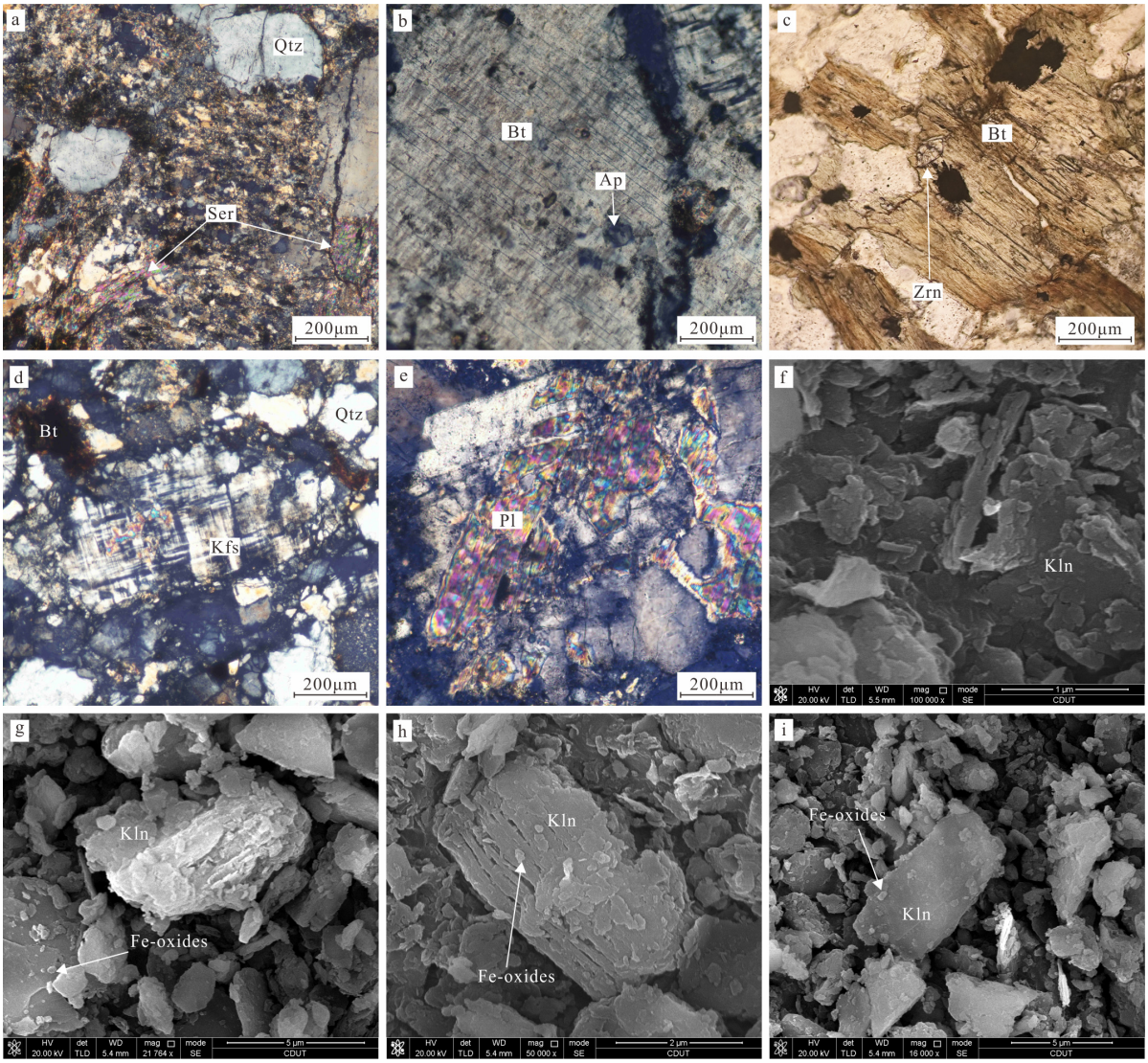

Figure 3. Photomicrograph showing the parent granite (**a**–**e**) and the regolith (**f**–**i**). (**a**) Aggregation of quartz + biotite alteration to muscovite and clay minerals; (**b**) biotite enclosing phosphatic granules; (**c**) biotite enclosing zircon grains; (**d**) quartz replacement of K-feldspar; (**e**) fragmented feldspar; (**f**–**i**) microscopic features of residual minerals and secondary minerals in the weathering crust, with spherical Fe-oxide attached to the surface of layered kaolinite. Abrrevitions: Qtz: Quartz, Kfs: K-feldspar, Bt: Biotite, Pl: Plagioclase, Ser: Sericite, Ap: Apatite, Zrn: Zircon.

Semi-quantitative XRD analysis (Figure 4) indicates that the mineral composition of the weathered crust mainly includes weathering residual detrital minerals (quartz, feldspar, mica) and secondary clay minerals (kaolinite, chlorite, illite, etc.). In terms of the entire

weathered crust, as the degree of weathering deepens, plagioclase, K-feldspar, and biotite are continuously decomposed, while the relative content of quartz gradually increases. There is an antagonistic relationship between feldspar minerals and clay minerals. Due to the weak weathering resistance of plagioclase, it is mostly completely decomposed in the partially weathered layer. The clay mineral content is highest in the fully weathered layer, and clay minerals can be observed in the weathered crust under scanning electron microscopy, mainly kaolinite, which has a loose structure and appears in schistose mineral aggregates, often forming complexes with Fe-oxides (Figure 3g–i).

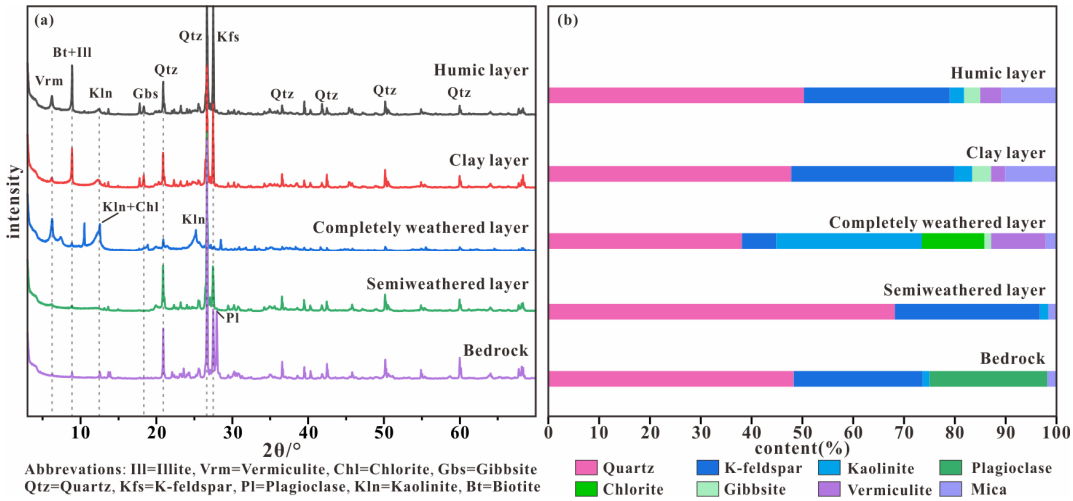

Figure 4. (**a**) XRD patterns of samples in the weathering crust and (**b**) mineral composition and content.

4.2. Major Elements

The results of the main element analysis for the samples are presented in Table 1. The rock exhibits an SiO_2 content ranging from 70.45% to 74.62%, K_2O content ranging from 4.52% to 6.02%, Na_2O content ranging from 2.55% to 3.13%, Fe_2O_3 content ranging from 2.34% to 3.71%, and MgO content ranging from 0.18% to 0.47%. It displays characteristics of high silica and alkali, low iron and magnesium, and is classified as a granite (Figure 5a), with some samples falling within the granodiorite range. Overall, it exhibits the features of high-K calc-alkaline granites (Figure 5b). The main elemental characteristics resemble those of the ion-adsorption type rare earth ore-forming granitic rocks found in the Mesozoic extensional structure of southern China [25].

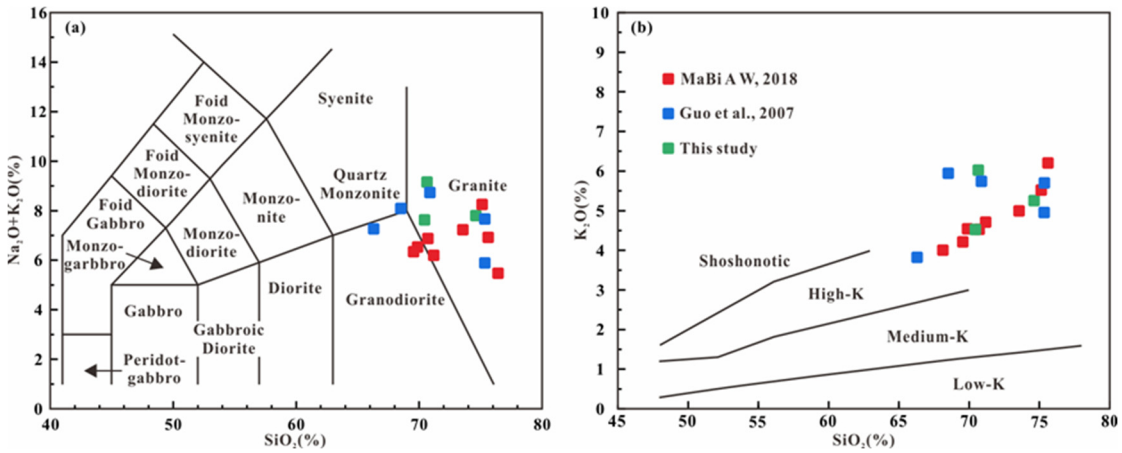

Figure 5. (**a**) $Na_2O + K_2O$ vs. SiO_2 [26], (**b**) K_2O vs. SiO_2 [19,20,27] diagrams for the Mosuoying granite.

4.3. Trace Elements

The diagrams (Figure 6) of primitive mantle normalized trace elements for the weathered crust samples reveal the following trends: The curves display a pronounced right-skewed pattern. The weathered crust demonstrates significant depletion of Ba, Nb, Sr, P, and Ti, while exhibiting enrichment of Rb, Th, U, La, Nd, and other elements. In comparison to the parent rock, most trace elements (Rb, Th, U, La, Y, Lu, etc.) are enriched in the weathered crust, except for Ba and Sr, which show depletion.

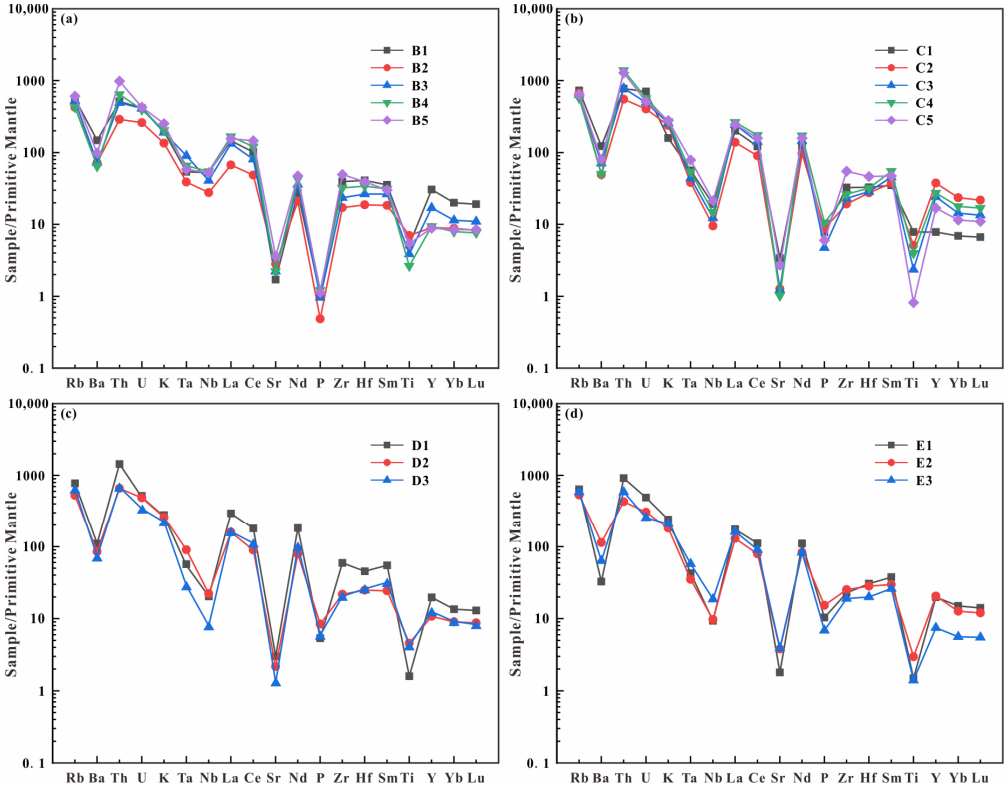

Figure 6. Primitive mantle-normalized elements diagrams for weathering crust samples [28]. (**a**) Clay layer; (**b**) completely layer; (**c**) semi-weathered layer; (**d**) bedrock layer.

4.4. Rees in Whole-Rock

The results of the rare earth element analysis in the weathered crust of the Mosuoying granite are shown in Table 2. The total rare earth element content in the bedrock ranges from 419.0 to 574.8 ppm, significantly higher than the lower limit of 150 ppm for rare earth ore-forming parent rocks, indicating a good rare earth mineralization foundation [29]. In the weathered crust, the rare earth elements in the humus layer and clay layer are lower than the average rare earth content in the bedrock, indicating varying degrees of loss. The fully weathered layer shows obvious enrichment of rare earth elements, with a content ranging from 517.1 to 803.0 ppm, higher than the ore-forming lower limit grade of 500 ppm [30], making it the main ore-bearing layer. The upper part of the partially weathered layer exhibits relative enrichment of rare earth elements, while the rare earth element content in the lower part is basically consistent with that of the bedrock.

The $(La/Yb)_N$ ratio in the weathered crust ranges from 5.9 to 29.0, while in the bedrock layer it ranges from 10.3 to 28.7, indicating significant differentiation of light and heavy rare earth elements in both the bedrock and weathered crust, with a similar degree of differentiation. The δEu value in the weathered crust ranges from 0.14 to 0.50, with an average of 0.28, which is consistent with the parent rock's δEu value (average 0.21). Both display a strong negative Eu anomaly. The δCe value in the weathered crust ranges

from 0.82 to 1.10, with an average of 0.89, which is similar to the parent rock's δCe value (average 0.85).

Overall, the rare earth elements in the weathered crust exhibit similar characteristics to those in the bedrock. The diagrams (Figure 7) of chondrite normalized rare earth distribution in each layer are inclined to the right, indicating that the overall composition of rare earth elements in the weathered crust is inherited from the bedrock and enriched during the weathering process.

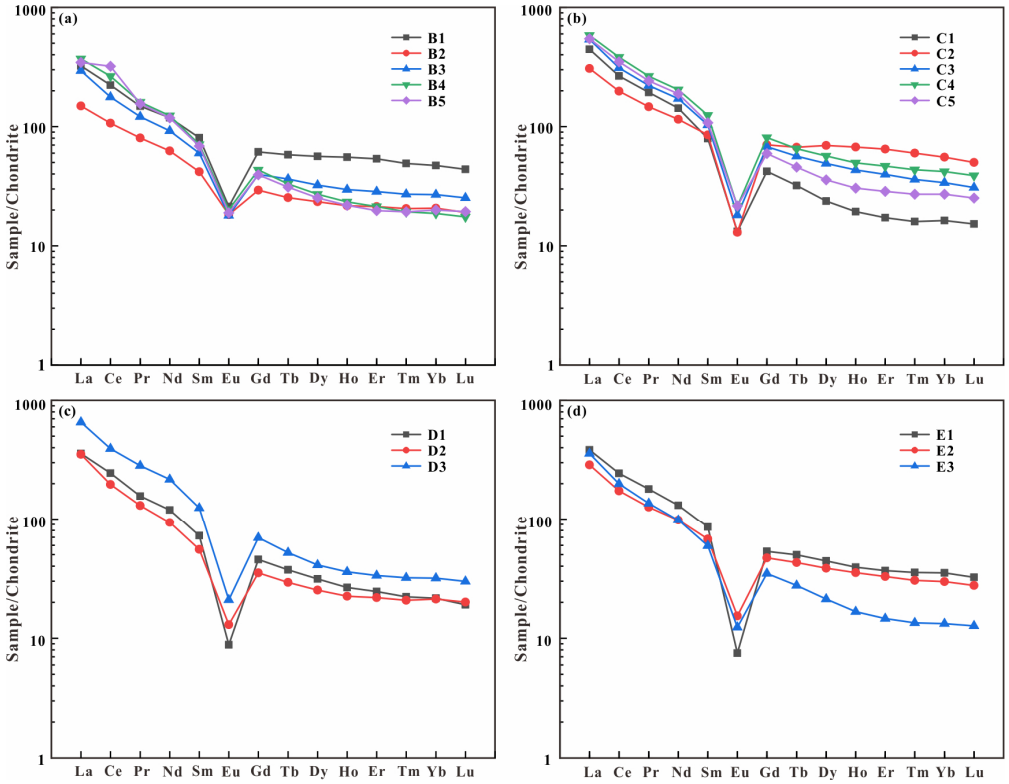

Figure 7. Chondrite-normalized REE patterns for weathering crust samples [28]. (**a**) Clay layer; (**b**) completely layer; (**c**) semi-weathered layer; (**d**) bedrock layer.

5. Discussion

5.1. Element Distrubution Characteristics

Previous studies have categorized major elements in the weathering process into three groups: (1) easily mobile elements, (2) movable elements, and (3) immobile elements [31]. Easily mobile elements: In comparison to the parent rock layer, the weathered crust exhibits significant losses of CaO and Na_2O, while the K_2O content remains generally consistent. The chemical index of alteration (CIA) gradually decreases from the humic layer to the bedrock layer. Movable elements: The SiO_2 content in the weathered crust shows depletion, with an overall increasing trend from the humic layer to the bedrock layer, reaching its lowest value in the clay layer. Immobile elements: The changes in immobile elements are more complex. The Al_2O_3 and Fe_2O_3 contents show enrichment and follow a similar trend, initially increasing and then decreasing from the humic layer to the bedrock layer, with accumulation in the clay layer. The TiO_2 content is enriched relative to the bedrock, displaying varying degrees of enrichment in each layer without a discernible pattern. The differences in MnO, P_2O_5, and MgO contents are minimal.

Trace elements are hosted in various minerals within rocks, with Zr, Ti, Hf, Ta, Nb, and other elements being typical conservative ones, often enriched in weathering-resistant accessory minerals such as zircon and sphene, which remain relatively stable during surface weathering [32]. An increase in such elements within the weathering crust may indicate the enrichment of the above-mentioned accessory minerals. The ratio of these elements

can be used to trace the origin of sediment [33]. The Nb/Ta ratio of the weathered crust samples is around 9, and the Zr/Hf ratio is around 35. These relatively stable ratios suggest that the weathering crust profile has a basically consistent origin, which is the result of the weathering of the original rock. Ba shares similar geochemical properties with K and is primarily found in potassium feldspar [34]. During weathering, potassium feldspar gradually depletes and decomposes with increasing weathering intensity, resulting in enhanced depletion of Ba. Sr is commonly associated with calcium-bearing minerals (plagioclase) and is considered a highly mobile element during weathering processes [35,36]. As weathering intensity intensifies, the loss of Sr becomes more prominent.

The diagrams (Figure 8) of the normalized REE pattern indicate that rare earth elements are enriched to varying degrees in each layer of the weathered crust. The ore-related granites show significantly higher contents of rare earth elements. Compared with the average value of Mosuoying granite, the granite associated with mineralization tends to have a relative enrichment of heavy rare earth elements.

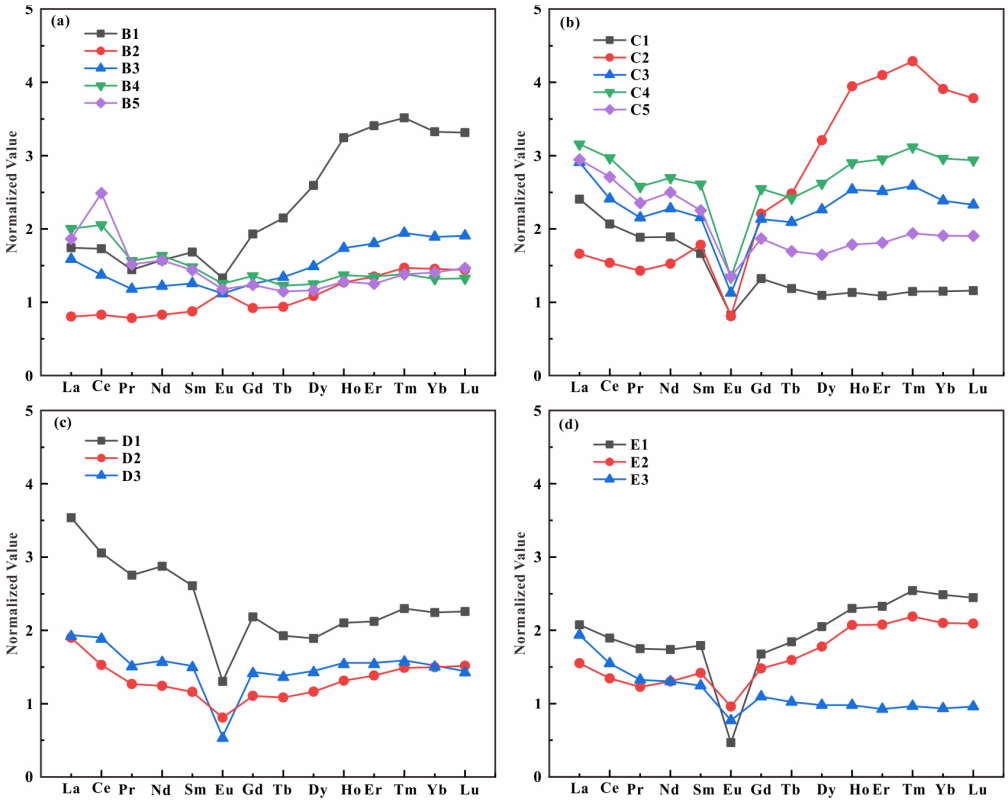

Figure 8. Normalized REE patterns for weathering crust samples. Normalized value = samples/average value of Mosuoying granite (date of this study and [19,20]). (**a**) Clay layer; (**b**) completely layer; (**c**) semi-weathered layer; (**d**) bedrock layer.

5.2. Bedrock Controls Mineralization

There are many types of ore-forming rocks for ion-adsorption type rare earth deposits, including granite, volcanic rock, metamorphic rock, carbonate rock, basalt, etc. [1,14,23,37]. Among them, granite has the widest distribution and highest research level among all ore-forming rocks. The ages of ore-forming granites for ion-adsorption type rare earth deposits in southern China vary widely, with distribution from the Ordovician to the Late Cretaceous [37–39]. Previous studies on the age of ore-forming granites suggest that the development of ion-adsorption type rare earth deposits in southern China has a certain preference for the formation time of the protolith, especially those closely related to early to middle Yanshanian intrusive intermediate-acidic granites [40,41]. Compared with previously discovered ion-adsorption type rare earth deposit protoliths, the formation

age of the Mosuoying granite is several hundred million years earlier, indicating that the formation of ion-adsorption type rare earth deposits is not influenced by the formation age of the protolith but rather by the characteristics of the rock.

Mosuoying granite exhibits high silica-alkali content and low iron-magnesium content. It is a highly differentiated S-type granite, with its magma derived from the partial melting of ancient crust and the incorporation of a small amount of mantle-derived magma [20]. During the partial melting process, LREE are more easily incorporated into the melt compared to HREE, and Eu tends to be retained in the solid phase [42]. When the degree of melting reaches 50%–70%, the residual phase consists of plagioclase + quartz + pyroxene + garnet + zircon. At this stage, the melted magma is enriched with easily fusible components, and light rare earth elements, potassium, sodium, silicon, and volatiles preferentially enter the melt in equilibrium with the residual phase [43]. Meanwhile, Eu exists in the forms of Eu^{3+} and Eu^{2+}, in which the ratio of Eu^{3+}/Eu^{2+} depends on oxygen fugacity [44]. Due to the larger ionic radius of Eu^{2+} (1.09 Å), it tends to substitute for high-coordinated Ca^{2+} (0.99 Å), Sr^{2+} (1.12 Å), and other cations in plagioclase, leading to its enrichment in the residual phase and depletion in the melt [45]. Therefore, the Mosuoying granite is characterized by enrichment in light rare earth elements and negative Eu anomalies.

The variation of major elements in the rock shows similarities to granites in South China. With increasing SiO_2 content, the contents of MgO, MnO, TiO_2, and CaO gradually decrease, while the REE content remains unaffected by changes in SiO_2 content (Figure 9). This indicates that the REE content is not constrained by magma differentiation, but magma differentiation does affect the migration and enrichment of LREE and HREE [46]. The REE distribution patterns in the basement rocks control the characteristics of rare earth elements in the weathering crust, and typically, the REE distribution pattern in the weathering crust is consistent with that of the basement rocks [47]. During the weathering process of S-type granite, a high P_2O_5 content (>0.08 wt.%) favors the formation of ion-adsorption type rare earth deposits, especially heavy rare earth deposits [48].

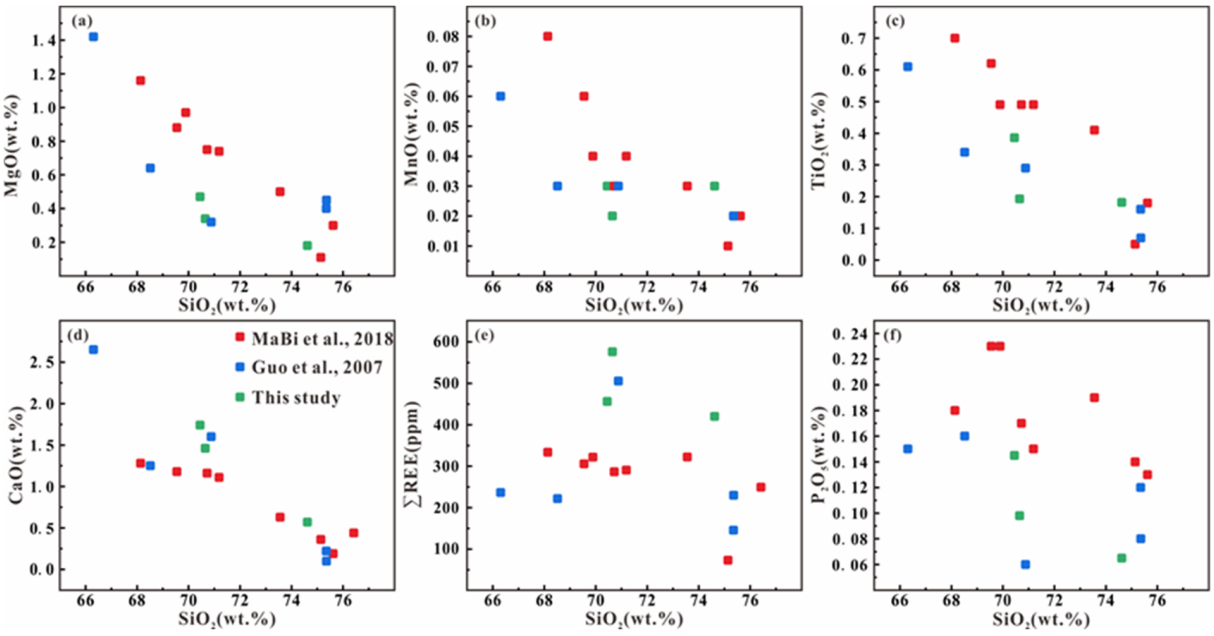

Figure 9. Harker diagrams for the Mosuoying granite [19,20].

Granitic rocks often undergo varying degrees of alteration due to post-magmatic processes, and hydrothermal alteration plays a crucial role in the later weathering and mineralization of parent rocks. Studies have shown that hydrothermal alteration plays a crucial role in the later weathering and mineralization of parent rocks. Common rare earth minerals found in granites include monazite, xenotime, apatite, and allanite. Hydrothermal

fluids not only bring in rare earth elements and increase their content in the parent rock [49], but also interact with weathering-resistant rare earth minerals such as monazite and xenotime, causing their dissolution and subsequent precipitation as easily weathered rare earth minerals such as apatite and allanite [50,51]. The altered bedrock in the study area has undergone greisenization, and compared to fresh bedrock, the chemical composition of the altered bedrock has significantly changed, particularly with a decrease in REE content, mainly in HREE. The ratio of LREE/HREE in the altered bedrock has increased from 2.64 and 3.56 to 7.39, which may be related to the dissolution and migration of apatite (containing HREE). During the process of weathering or alteration of rocks, apatite can be chemically dissolved due to hydrothermal activity. As apatite dissolves, it releases the REEs it contains, including both LREEs and HREEs. Some of the REEs may remain in the proximity of the dissolved apatite and precipitate in situ, forming secondary minerals such as monazite and xenotime [52]. These secondary minerals can still retain a portion of the REEs that were originally contained in the apatite. However, the monazite and xenotime formed in situ are highly resistant to weathering and remain mostly unchanged in the completely weathered layer. As a result, they cannot provide the necessary ionic rare earth elements for ore formation, hindering the development of rare earth deposits. On the other hand, some of the REEs released from the dissolved apatite can migrate along with hydrothermal fluids [52]. This migration can result in the loss of these REEs from the rock system, leading to a decrease in the overall rare earth content within the bedrock. As the main component of HREEs in the bedrock, the loss of these REEs leads to a significant decrease in the content of HREEs in the bedrock, thereby reducing the material basis for weathering and mineralization. In contrast to previous views, the alteration of the Mosuoying granite restricts the possibility of weathering mineralization, suggesting that the influence of basement rock alteration on rare earth mineralization is not uniform.

5.3. Migration and Enrichment Patterns of Elements

The migration characteristics of substances in open geological systems are commonly assessed using mass balance calculation methods, including the composition-volume diagram method [53], quantitative calculation method [54,55], isocon diagram method [56], normalized isocon diagram method [57], among others. In this study, considering the involvement of multiple components in the migration and enrichment of the open system (weathered profile), the normalized isocon diagram method was selected. This method highlights the continuous changing trend of active components and explores the migration and enrichment characteristics of elements in granite-weathered profiles. The method adjusts all the isocons (defined by unaltered and altered sample pairs) to a normalized isocon, modifies the active components according to the adjustment ratio, and provides information on substance transfer. Its core lies in the determination of immobile components [56–58]. For silica-bearing geological bodies, Zr exhibits highly stable properties. However, in granite, the majority of Zr is present in zircon, with a low overall content and uneven distribution throughout the rock. Treating it as an immobile component may introduce gross errors between samples. In contrast, TiO_2 is evenly distributed and rarely loses during weathering. Therefore, TiO_2 was selected as the immobile component for calculating the mass balance of material migration. The results are shown in Figure 10.

The enrichment characteristics of rare earth elements were determined using the enrichment factor (R), calculated by the formula $R = Cx/Cp$, where Cx represents the content of rare earth elements in the sample and Cp represents the content of rare earth elements in the parent rock. The calculation results are presented in Table 3.

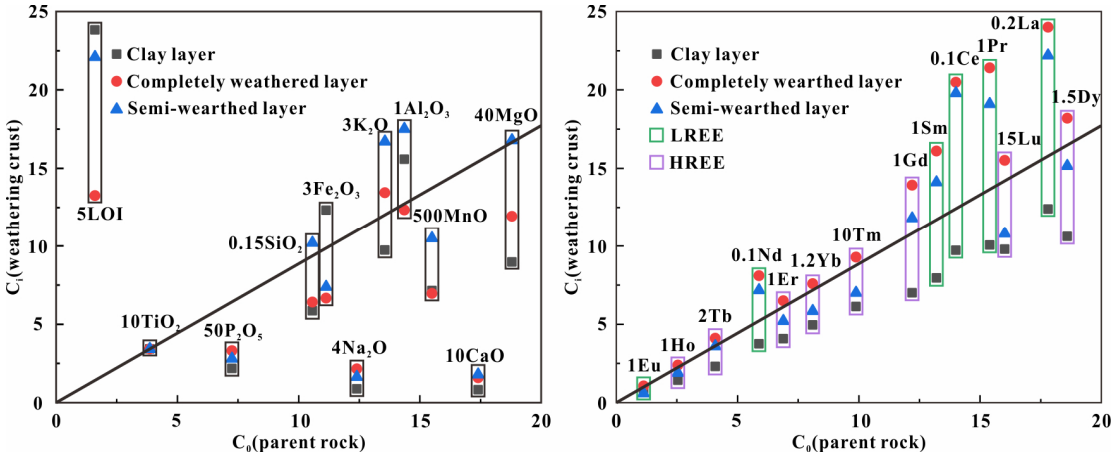

Figure 10. Normalized isocon diagrams for the weathering crust. The thick line indicates the unified isocon defined by TiO_2; the numbers before the oxide and element symbol represent the scaling coefficients.

Table 3. REE enrichment factor.

	B/C	B/D	B/E	C/D	C/E	D/E
La_2O_3	0.58	0.62	0.82	1.06	1.41	1.33
Ce_2O_3	0.60	0.65	0.89	1.08	1.47	1.36
Pr_2O_3	0.62	0.70	0.91	1.12	1.45	1.29
Nd_2O_3	0.63	0.72	0.94	1.15	1.50	1.31
Sm_2O_3	0.64	0.77	0.91	1.19	1.41	1.19
Eu_2O_3	1.09	1.37	1.65	1.26	1.51	1.20
Gd_2O_3	0.66	0.85	0.95	1.28	1.42	1.11
Tb_2O_3	0.69	0.93	0.92	1.34	1.33	1.00
Dy_2O_3	0.70	1.01	0.95	1.44	1.35	0.94
Ho_2O_3	0.73	1.08	1.01	1.49	1.38	0.93
Er_2O_3	0.74	1.09	1.04	1.48	1.40	0.95
Tm_2O_3	0.75	1.10	1.03	1.48	1.37	0.93
Yb_2O_3	0.76	1.07	1.02	1.41	1.34	0.95
Lu_2O_3	0.77	1.09	1.03	1.42	1.33	0.94

B: clay layer, C: completely weathered layer, D: semi-weathered layer, E: bedrock.

The normalized isocon diagram demonstrates that different major elements in each layer of the weathered crust exhibit varying degrees of migration relative to the bedrock layer. The migration and enrichment patterns of these elements are not consistent but are influenced by the inherent nature of the elements themselves and the surrounding environment. From the bedrock layer to the semi-weathered layer, components such as P_2O_5, Fe_2O_3, Na_2O, MnO, and CaO were lost, while SiO_2, K_2O, Al_2O_3, and other components were gained. From the semi-weathered layer to the completely weathered layer, most major elements were lost, with P_2O_5 and Na_2O gained. From the completely weathered layer to the clay layer, significant changes occur in Fe_2O_3, K_2O, Al_2O_3, and MgO. Fe_2O_3 and Al_2O_3 migrate inwards, while MgO and K_2O migrate outwards. The content of Fe_2O_3 is influenced by redox conditions, as Fe^{2+} easily oxidizes to Fe^{3+} under surface conditions, leading to the enrichment of Fe_2O_3. The migration of easily soluble components such as CaO, Na_2O, P_2O_5, and K_2O is related to the loss of ions such as Ca^{2+}, Na^+, and K^+ during weathering processes [59].

The migration of rare earth elements follows a distinct pattern. The normalized isocon diagram indicates that the migration and enrichment patterns of all rare earth elements in the weathered layer are consistent, albeit with varying enrichment factors. From the semi-weathered layer to the fully weathered layer, all rare earth elements were gained to different extents, leading to their enrichment in the completely weathered layer. From the completely weathered layer to the clay layer, all rare earth elements were lost in substantial

quantities, resulting in significant depletion of these elements compared to the bedrock layer and semi-weathered layer. This indicates that in this layer, the adsorption capacity of clay minerals for rare earth elements is smaller than the leaching effect of weathering, causing the migration of rare earth elements. Two factors influence this phenomenon: firstly, the increase in Fe^{3+} in this layer, as Fe^{3+} easily forms $Fe(OH)_3$ and aggregates with clay minerals, thereby reducing the adsorption capacity of clay minerals for rare earth elements; secondly, the relatively intense weathering in this layer causes a decrease in the surface void structure of clay minerals [60], resulting in a lower adsorption capacity of clay minerals for rare earth elements compared to the fully weathered layer. During the migration process, the extent of migration for light and heavy rare earth elements is influenced by the iron oxide–clay mineral composites in the weathering shell. Clay minerals [61] and Fe-oxides [62] are the main carriers of ion-exchangeable and Fe-oxide-bound REE, respectively, and they play a certain controlling role in the differentiation and enrichment of rare earth elements. The iron oxide-clay mineral composites formed are favorable for the enrichment of heavy rare earth elements in the weathering crust [63]. Iron oxides, especially crystalline iron oxides, exhibit selective adsorption towards heavy rare earth elements [62], promoting the formation of heavy rare earth minerals. However, the limited presence of iron oxide–clay mineral composites in the weathering crust of the Mosuoying granite is insufficient to alter the characteristics of light rare earth element distribution in the bedrock itself, resulting in a higher migration extent for LREE compared to HREE in the profile.

6. Conclusions

(1) The deposit type is characterized by a distribution of light rare earth elements, with the fully weathered layer serving as the primary ore-bearing horizon. The vertical distribution of REEs exhibits a pattern of "low-high-low".
(2) The REE characteristics in the weathered crust are controlled by the parent rock. Magmatic differentiation does not affect the REE content of the parent rock, while hydrothermal alteration reduces the overall REE content and increases the LREE/HREE ratio, which is unfavorable for mineralization, especially HREE mineralization.
(3) The migration characteristics of elements indicate that the distribution of major elements in the weathering crust is influenced by the properties of the elements themselves and the surrounding environment, while rare earth elements exhibit regular migration patterns. From the semi-weathered layer to the completely weathered layer, all rare earth elements were gained, while from the completely weathered layer to the clay layer, all rare earth elements were lost.

Author Contributions: Writing—original draft preparation, L.G. and Y.G.; methodology, Y.L.; writing—review and editing, B.Y. and L.G.; resources, C.Y.; supervision, D.D. and S.T.; data curation, L.Z. and H.J. All authors have read and agreed to the published version of the manuscript.

Funding: State Key Laboratory of Ore Deposit Geochemistry of China (SKLODG grant #202007); Sichuan Provincial Government Invested Geological Exploration Project (DZ202015).

Data Availability Statement: Data are contained within the article.

Acknowledgments: The State Key Laboratory of Ore Deposit Geochemistry provided by Guiyang Institute of Geochemistry, thanks to the units and individuals for the help of this article.

Conflicts of Interest: Bing Yan has received research grants from the State Key Laboratory of Ore Deposit Geochemistry. The funding sponsors had no role in the design of the study; in the collection, analyses, or interpretation of data; in the writing of the manuscript, and in the decision to publish the results.

References

1. Sanematsu, K.; Watanabe, Y. Characteristics and genesis of ion adsorption-type rare earth element deposits. *Rev. Econ. Geol.* **2016**, *18*, 55–79.
2. Foley, N.; Ayuso, R.; Hubbard, B.; Bern, C.; Shah, A. Geochemical and Mineralogical Characteristics of REE in Granite-Derived Regolith of the Southeastern United States. *Miner. Resour. A Sustain. World* **2015**, *S1–S5*, 725–728.
3. Yang, B.Q.; Zhang, X.P. Analysis of Global Rare Earth Production and Consumption Structure. *Chin. Rare Earth.* **2014**, *35*, 110–118.
4. Riesgo García, M.V.; Krzemień, A.; Manzanedo del Campo, M.Á.; Álvarez, M.M.; Gent, M.R. Rare earth elements mining investment: It is not all about China. *Resour. Pol.* **2017**, *53*, 66–76. [CrossRef]
5. Padrones, J.T.; Imai, A.; Takahashi, R. Geochemical behavior of rare earth elements in weathered granitic rocks in Northern Palawan, Philippines. *Resour. Geol.* **2017**, *67*, 231–253. [CrossRef]
6. Ci, R.A.; Wang, D.Z. *Rare Earth Beneficiation and Extraction Technology*; Science Press: Beijing, China, 1996.
7. Zhang, W.; Chen, W.; Mernagh, T.P.; Zhou, L. Quantifying the nature of ore-forming fluids in the Dalucao carbonatite-related REE deposit, Southwest China: Implication for the transport and deposition of REEs. *Miner. Depos.* **2022**, *57*, 935–953. [CrossRef]
8. Weng, Q.; Yang, W.B.; Niu, H.C.; Li, N.B.; Roger, H.M.; Zurevinski, S.; Wu, D. Formation of the Maoniuping giant REE deposit: Constraints from mineralogy and in situ bastnäsite U-Pb geochronology. *Am. Mineral.* **2022**, *107*, 282–293. [CrossRef]
9. Chen, C.J.; Deng, Z.X.; Wu, Q.H.; Yan, L.J.; She, Z.M.; Yan, Z.A. Metallogenic Conditions and Ore—Search Prospect of the Xinpaoshan Ion-Adsorption Type Rare-Earth Deposit in the Yingjiang Area, Western Yunnan. *Geol. Explor.* **2021**, *57*, 751–761.
10. Fan, G.Q.; Qin, Y.L.; Zhan, H.Y.; Xiong, C.L.; Chen, D.Y.; Huang, S.F.; Peng, Y. Metallization regularity and prospecting target area in Panzhihua—Xichang area of Sichuan Province. *Chin. Geol. Sur.* **2022**, *9*, 23–31.
11. Luo, X.Y. Metallogenic conditions and formation mechanism of ion adsorption rare earth deposits in Hunan Province. *Acta Mineral. Sin.* **2011**, *A1*, 332–333.
12. Liu, B.; Long, G.Y.; Fu, Y.R.; Yun, P. Metallogenic regularity and new exploration finding of the ion-adsorption type REE deposits in Hainan Island. *Miner. Resour. Geol.* **2017**, *31*, 300–305.
13. 17 newly discovered ion adsorption type light rare earth mineralization sites in Anhui Province. *Rare Earth Inf.* **2018**, *3*, 18.
14. Zhao, Z.; Wang, D.H.; Wang, C.H.; Wang, Z.; Zou, X.Y.; Feng, W.J.; Zhou, H.; Huang, X.P.; Huang, H.G. Progress in prospecting and research of ion-adsorption type REE deposits. *Acta Geosci. Sinica.* **2019**, *93*, 1454–1465.
15. Xia, X.H.; Liu, T.Q.; Yin, C.; Duan, L.; Yang, W.; Tan, H.Q.; Zhou, J.Y.; Wang, C.H. First discovery of ion adsorption-type (medium—Heavy) REE depositin the Panzhihua—Xichang area, Sichuan Province, and its significance. *Geol. Rev.* **2022**, *68*, 1540–1543.
16. Zou, J.Z.; Nie, F.; Guo, J.C. New discovery of ion-absorption type REE mineral occurrence in the Mianning-Dechang area, Sichuan Province. *Geol. China.* **2023**, *50*, 648–649.
17. Xia, X.H.; Liu, T.Q.; Yin, C.; Duan, L.; Yang, W.; Wang, C.; Li, N.; Wang, C.H.; Tan, H.Q. Geological characteristics and metallogenic factors of the Kuanyu ion adsorption REE deposit in the Panzhihua-Xichang district, Sichuan Province, SW China. *Geol. China.* **2021**. Available online: https://kns.cnki.net/kcms/detail/11.1167.P.20210809.002.html (accessed on 22 September 2023).
18. Hou, Z.Q.; Tian, S.H.; Xie, Y.L. The Himalayan Mianning-Dechang REE belt associated with carbonatite-alkaline complexes, eastern Indo-Asian collision zone, SW China. *Ore Geol. Rev.* **2009**, *36*, 65–89. [CrossRef]
19. Mabi, A.W.; Yang, Z.X.; Zhang, M.C.; Wen, D.K.; Li, Y.L.; Liu, X.Y. Two Types of Granites in the Western Yangtze Block and Their Implications for Regional Tectonic Evolution: Constraints from Geochemistry and Isotopic Data. *Acta Geosci. Sinica.* **2018**, *92*, 89–105. [CrossRef]
20. Guo, C.L.; Wang, D.H.; Chen, Y.C.; Zhao, Z.G.; Wang, Y.B.; Fu, X.F.; Fu, D.M. SHRIMP U-Pb zircon ages and major element, trace element and Nd-Sr isotope geochemical studies of a Neoproterozoic granitic complex in western Sichuan: Petrogenesis and significance. *Acta Petro. Sin.* **2007**, *23*, 2457–2470.
21. Li, Y.H.M.; Zhao, W.W.; Zhou, M.F. Nature of parent rocks, mineralization styles and ore genesis of regolith-hosted REE deposits in South China: An integrated genetic model. *J. Asian Earth Sci.* **2017**, *148*, 65–95. [CrossRef]
22. Hou, Z.Q.; Ma, H.W.; Zaw, K.; Zhang, Y.Q.; Wang, M.J.; Wang, Z.; Pan, G.T. The Himalayan Yulong porphyry copper belt: Product of large-scale strike-slip faulting in eastern Tibet. *Econ. Geol.* **2003**, *98*, 125–145.
23. Zhou, M.F.; Li, X.X.; Wang, Z.C.; Li, X.C.; Liu, J.C. The genesis of regolith-hosted rare earth element and scandium deposits: Current understanding and outlook to future prospecting. *Chin. Sci. Bull.* **2020**, *65*, 3809–3824. [CrossRef]
24. Lu, L.; Liu, Y.; Liu, H.C.; Zhao, Z.; Wang, C.H.; Xu, X.C. Geochemical and Geochronological Constraints on the Genesis of Ion-Adsorption-Type REE Mineralization in the Lincang Pluton, SW China. *Minerals* **2020**, *10*, 1116. [CrossRef]
25. Zhao, X.; Li, N.B.; Huizenga, J.M.; Yan, S.; Yang, Y.Y.; Niu, H.C. Rare earth element enrichment in the ion-adsorption deposits associated granites at Mesozoic extensional tectonic setting in South China. *Ore Geol. Rev.* **2021**, *137*, 104317. [CrossRef]
26. Eric, A.K. Middlemost. Naming materials in the magma/igneous rock system. *Earth Sci. Rev.* **1994**, *37*, 215–224.
27. Peccerillo, A.; Taylor, S.R. Geochemistry of eocene calc-alkaline volcanic rocks from the Kastamonu area, Northern Turkey. *Contrib. Mineral. Petrol.* **1976**, *58*, 63–81. [CrossRef]
28. Sun, S.-S.; McDonough, W.F. Chemical and isotopic systematics of oceanic basalts: Implications for mantle composition and processes. *Geol. Soc. Lond. Spec. Publ.* **1989**, *42*, 313–345. [CrossRef]
29. Bai, G.; Wu, C.Y.; Ding, X.S.; Yuan, Z.X.; Huang, D.H.; Wang, P.H. *Forming Conditions and Distribution Regularity of Ionic Rare Earth Deposits in the Nanling Area*; Institute of Deposit Geology, Ministry of Geology and Mineral Resources: Beijing, China, 1989; pp. 1–105.

30. Bao, Z.W.; Zhao, Z.H. Geochemistry of mineralization with exchangeable REY in the weathering crusts of granitic rocks in South China. *Ore Geol. Rev.* **2008**, *33*, 519–535. [CrossRef]
31. Huang, Z.G.; Zhang, W.Q.; Chen, J.H.; Liu, R.H. *Red Weathering Crust in Southern China*; China Ocean Press: Beijing, China, 1996.
32. Adi, M.; Kotaro, Y.; Koichiro, W. Geochemistry of Rare Earth Elements(REE) in theWeathered Crusts from the Granitic Rocks in Sulawesi Island, Indonesia. *J. Earth Sci.* **2014**, *25*, 460–472.
33. Schwarz, T. Distribution and genesis of bauxite on the Mambilla Plateau. SE Nigeria. *Appl. Geochem.* **1997**, *12*, 119–131. [CrossRef]
34. Xie, M.J.; Zhou, J.; Wang, X.Q.; Qi, F.Y.; Zhang, B.M.; Wu, H.; Liu, D.S.; Liu, Y.H.; Liu, F.T. Research of Elements′ Migration and Enrichment Characteristics of Ion-adsorption Type REE Deposits in Southern Jiangxi Province. *J. Chin. Rare Earth Soc.* **2022**, *40*, 697–710.
35. San, F.X.; Ling, W.L.; Hu, Y.H.; Xie, S.Y. Element and Sr-Nd isotopic geochemistry profiles of weathered dioritic rocks in the eastern Three Gorges and its implication. *Geochemica* **2013**, *42*, 430–446.
36. Cao, W.J.; Ji, H.B.; Zhu, X.F.; Zhao, X.Y.; Qiao, M.M. Contrast of geochemical features of typical weathered profiles in Guizhou Plateau. *Carsologica Sin.* **2012**, *31*, 131–138.
37. Zhao, Z.; Wang, D.H.; Chen, Z.Y.; Guo, N.X.; Liu, X.X.; He, H.H. Metallogenic Specialization of Rare Earth Mineralized Igneous Rocks in the Eastern Nanling Region. *Geotecton. Metallog.* **2014**, *38*, 255–263.
38. Wang, D.H.; Zhao, Z.; Yu, Y.; Wang, C.H.; Dai, J.J.; Sun, Y.; Zhao, T.; Li, J.K.; Huang, F.; Chen, Z.L.; et al. A Review of the Achievements in the Survey and Study of Ion-absorption Type REE Deposits in China. *Acta Geosci. Sin.* **2017**, *38*, 317–325.
39. Ming, T.X.; Xue, G.; Tang, Z.; Yang, Q.B.; Li, X.M.; Bai, Y.; Su, X.Y. Distribution Characteristics and Geological Significance of R are Earth Oxides in Weathered Crust of Pinghe Granite, Western Yunnan. *J. Chin. Rare Earth Soc.* **2021**, *39*, 644–652.
40. Fu, W.; Zhao, Q.; Luo, P.; Li, P.Q.; Lu, J.P.; Zhou, H.; Yi, Z.B.; Xu, C. Mineralization diversity of ion-adsorption type REE deposit in southern China and the critical influence of parent rocks. *Acta Geosci. Sin.* **2022**, *96*, 3901–3925.
41. Zhang, L.; Wu, K.X.; Chen, L.K.; Zhu, P.; Ouyang, H. Overview of Metallogenic Features of Ion-adsorption Type REE Deposits in Southern Jiangxi Province. *J. Chin. Soc. Rare Earths* **2015**, *33*, 10–17.
42. Yang, R.Y.; Huang, Z.X.; Lu, D.F. Trace element geochemistry of granite in the Panxi region. *Sci. Sin. Chim.* **1988**, *2*, 183–192.
43. Yang, X.M.; Zhang, P.S. Geochemical characteristics and petrogenetic significance of rare earth elements in the Guposhan granite complex. *J. Chin. Rare Earth Soc.* **1991**, *1*, 70–75.
44. Hanson, G.N. Rare earth elements in petrogenetic studies of igneous systems. *Ann. Rev. Earth Planet. Sci.* **1980**, *8*, 371–406. [CrossRef]
45. Wang, J.M.; Ding, C.G. The negative Eu anomaly of feldspar in Suzhou A-type granite and its origin significance. *Rock. Miner. Anal.* **1995**, *11*, 108–112.
46. Lu, L.; Wang, C.H.; Wang, D.H.; He, G.W.; Sun, Y. Constrains on metallogenic mechanism of ion-adsorption type REE deposit from mineralogy, geochemistry and chronology of Banggunjianshan granite, Yunnan Province. *Acta Geol. Sin.* **2023**, *97*, 1494–1507.
47. Ci, R.A.; Tian, J. *Weathering Crust Leaching Type Rare Earth Ore Chemical Metallurgy*; Science Press: Beijing, China, 2006.
48. Fu, W.; Li, X.T.; Feng, Y.Y.; Feng, M.; Peng, Z.; Yu, H.X.; Lin, H. Chemical weathering of S-type granite and formation of Rare Earth Element (REE)-rich regolith in South China: Critical control of lithology. *Chem. Geol.* **2019**, *520*, 33–51. [CrossRef]
49. Xu, C.; Kynicky, J.; Smith, M.P.; Kopriva, A.; Brtnicky, M.; Urubek, T.; Yang, Y.H.; Zhao, Z.; He, C.; Song, W.L. Origin of heavy rare earth mineralization in South China. *Nat. Commun.* **2017**, *8*, 14598. [CrossRef]
50. Bern, C.R.; Yesavage, T.; Foley, N.K. Ion-adsorption REEs in regolith of the Liberty Hill pluton, South Carolina, USA: An effect of hydrothermal alteration. *J. Geochem. Explor.* **2017**, *172*, 29–40. [CrossRef]
51. Li, M.Y.H.; Zhou, M.F.; Williams-Jones, A.E. The genesis of regolith-hosted heavy rare earth element deposits: Insights from the world-class Zudong deposit in Jiangxi Province, South China. *Econ. Geol.* **2019**, *114*, 541–568. [CrossRef]
52. Huang, Y.F.; Tan, W.; Bao, Z.W.; He, H.P.; Liang, X.L.; Huang, J.; Wang, H. Constraints of parent rock on the formation of ion adsorption HREE deposit in the weathering crust of the Shangyou graint batholith. *Geotecton. Metallog.* **2022**, *46*, 303–317.
53. Gresens, R.L. Composition-volume relationships of metasomatism. *Chem. Geol.* **1967**, *2*, 47–55. [CrossRef]
54. Nesbitt, H.W. Mobility and fractionation of rare earth elements during weathering of a granodiorite. *Nature.* **1979**, *279*, 206–210. [CrossRef]
55. George, H.B.; William, E.D. Constitutive mass balance relations between chemical composition, volume, density, porosity, and strain in metasomatic hydrochemical systems: Results on weathering and pedogenesis. *Geochim. Cosmochim. Acta* **1987**, *51*, 567–587.
56. Grant, J.A. The Isocon diagram. A simple solution to Gresens' equation for metasomatic alteration. *Econ. Geol.* **1986**, *81*, 1976–1982. [CrossRef]
57. Guo, S.; Ye, K.; Chen, Y.; Liu, J.B. A normalization solution to mass transfer illustration of multiple progressively altered samples using the isocon diagram. *Econ. Geol.* **2009**, *104*, 881–886. [CrossRef]
58. Guo, S.; Ye, K.; Chen, Y.; Liu, J.B.; Zhang, L.M. Introduction of mass-balance calculation method for component transfer during the opening of a geological system. *Acta Petro. Sin.* **2013**, *29*, 1486–1498.
59. Zhang, B.; Zhu, X.P.; Zhang, B.H.; Gao, R.D.; Zeng, Z.J.; Ma, G.T. Geochemical Characteristics of Tuguanzhai Ion-Adsorption Type REE Deposit in Tengchong, Yunnan. *J. Chin. Rare Earth Soc.* **2019**, *37*, 491–506.
60. Li, M.; Zhou, M.F. The role of clay minerals in forming the regolith-hosted heavy rare earth element deposits. *Am. Mineral.* **2020**, *105*, 92–108. [CrossRef]
61. Zhou, J.M.; Yuan, P.; Yu, L.; Liu, X.Y.; Zhang, B.F.; Fan, W.X.; Liu, D. Mineralogical characteristics of fine particles of the tuff weathering crust from the Bachi rare earth element (REE) deposit. *Acta Mineral. Sin.* **2018**, *38*, 420–428.

62. Wu, P.Q.; Zhou, J.W.; Huang, J.; Lin, X.J.; Liang, X.L. Enrichment and fractionation of rare earth elements in ion-adsorption rare earth elements deposits: Constraints of iron oxide-clay mineral composites. *Geochimica* **2022**, *51*, 271–282.
63. Quinn, K.A.; Byrne, R.H.; Schijf, J. Sorption of yttrium and rare earth elements by amorphous ferric hydroxide: Influence of pH and ionic strength. *Mar. Chem.* **2006**, *99*, 128–150. [CrossRef]